Int. J. Electrochem. Sci., 16 **(2021)** Article ID: 210764, doi: 10.20964/2021.07.13

International Journal of
ELECTROCHEMICAL
SCIENCE
www.electrochemsci.org

Study on Improving Corrosion Resistance of Tantalum Coating by Anodic Oxidation

Jincheng Hou[1], *Yuan Wang*[1,*], *Zhentao Yuan*[2,*], *Hongzhong Cai*[3,*], *Wengang Chen*[1]

[1] School of Machinery and Communications, Southwest Forestry University, Kunming, 650224, China;
[2] City college, Kunming University of Science and Technology, Kunming, 650093, China; 3. Kunming Institute of Precious Metals, Kunming, 650106, China.
[*]E-mail: wyuan88@126.com, kmust_welding@163.com, chz@ipm.com.cn

Received: 9 March 2021 / *Accepted:* 18 april 2021 / *Published:* 31 May 2021

Tantalum (Ta) coatings have been widely used as a corrosion-resistant material in the aerospace, weapon equipment, and nuclear industries. However, the widespread use of these coatings is hindered mainly by selective corrosion. In this work, the selective corrosion of Ta coatings is reduced via anodic oxidation. The microstructure and thickness of the coatings were evaluated through scanning electron microscopy (SEM) and X-ray photoelectron spectroscopy (XPS) depth profiles. Moreover, XPS was also used to determine the valence state and surface composition of the coatings. Furthermore, the corrosion-resistance behavior of the coating was investigated using an electrochemical workstation. The results revealed that the oxide film on the surface of the coating was still Ta_2O_5 after anodization, and the film thickness (i.e., 150 nm) was approximately five times greater than that of the natural oxide. Furthermore, the anodic oxidation process reduced the formation of an island structure, improved the compactness of the Ta coating, and reduced chloride ion transport. More importantly, the corrosion current density of the Oxide/Ta/Mo (anodic oxidation) coating decreased by 26.47% (from 0.034 $A{\cdot}cm^{-2}$ to 0.025 $A{\cdot}cm^{-2}$) and the self-corrosion potential increased by 36.84% (from -0.38 V to -0.24 V). This work can serve as a reference for improving the corrosion resistance of Ta coatings.

Keywords: tantalum coating; anodic oxidation; corrosion resistance; selective corrosion

1. INTRODUCTION

Tantalum (Ta) coatings have attracted increasing attention in the aerospace, weapon equipment, and nuclear industries, due to their high corrosion resistance, high temperature stability, and excellent biocompatibility [1–3].

However, these coatings are quite susceptible to selective corrosion, where the natural oxide film is easily destroyed during usage [4]. Various attempts have been made to solve this problem. Many studies have shown that plastic deformation, barrier protection, and anodic oxidation are simple and effective in reducing the selective corrosion of materials [5–7]. Ma et al. [5] showed that cold rolling deformation had a dual effect on the corrosion resistance of the alloy. High strain rolling deformation increased the corrosion resistance and low strain rolling has the opposite effect. Asgari et al. [6] investigated the corrosion resistance of coatings by considering barrier protection, which depends strongly on the zinc layer chemical composition.

Compared with plastic deformation and barrier protection, anodic oxidation is a common and simple surface treatment method, where an electrochemical treatment leads to the formation of a substantial uniform corrosion-resistant film [8–11]. The effect of anodic oxidation on the corrosion resistance of aluminum and titanium alloys has been extensively investigated. For example, Wang et al. [12] showed that this treatment can lead to a significant improvement in the thickness and density of an oxide film. This indicated that an electrochemical treatment can change the growth of the film, thereby forming a substantial uniform corrosion-resistant film. Zubillaga et al. [13] investigated the corrosion protection of anodic alumina films, and found that the adhesion performance of these films improved after anodization. Ingrid et al. [14] reported that anodic oxidation can improve the polarization resistance and reduce the corrosion current density, thereby improving the corrosion resistance. Nevertheless, plastic deformation and barrier protection yield improvements in the oxide film associated with the corrosion resistance. Including an appropriate anodic oxidation treatment in the treatment processes will reduce or even eliminate the negative effect of Ta on selective corrosion. However, the mechanisms governing selective corrosion are still unknown, and hence controlling this corrosion is difficult.

In this work, we formed an anodic oxide film on the Ta coating surface using an anodization process. The microstructure of this film was determined via scanning electron microscopy (SEM). Similarly, the chemical composition was determined by means of X-ray photoelectron spectroscopy (XPS) and XPS depth profiling. Subsequently, the corrosion characteristics and properties of the oxide film were investigated by obtaining the polarization curves and performing electrochemical impedance spectroscopy (EIS) measurements.

2. EXPERIMENTAL AND COMPUTATIONAL DETAILS

2.1 Preparation of Ta coating on Mo

Ta coatings were prepared by means of chemical vapor deposition (CVD) using a vertical tube reactor. The raw materials used were a Ta plate (≥ 99.99 wt.%) and Mo plate (60 mm×40 mm×30 mm), and the oxidation gas and reducing gas were, respectively, Cl_2 and H_2 with a purity of more than 99.9%. The chlorination chamber and the surface treatment substrate were heated using an electric furnace and a medium frequency induction furnace, respectively. During the deposition process, the pressure in the deposition chamber was maintained at ~105 Pa, and the flow rates of Cl_2 and H_2 were 50–200 mL/min and 400–600 mL/min, respectively. The total thickness of the Ta coating was ~2 mm. The substrate (Mo plate) and the deposited material (Ta coating) were separated by means of wire cutting and chemical etching(The samples marked as Ta/Mo). A schematic showing the CVD preparation of the coating is presented in Figure 1.

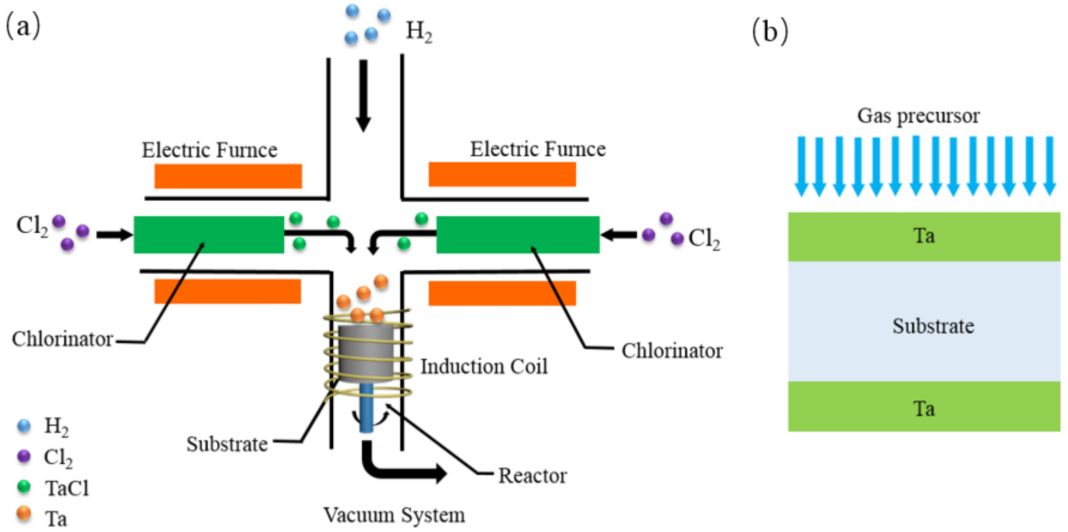

Figure 1. Schematic of tantalum coating prepared via chemical vapor deposition (CVD) (a) and structure of the coating (b).

The main reactions that occur during the CVD process are as follows:

$$2Ta + 5Cl_2(g) \rightarrow 2TaCl_5 \quad (1)$$

$$2TaCl_5 + 5H_2(g) \rightarrow 2Ta + 10HCl(\mathrm{g}) \quad (2)$$

2.2 Anodic oxidation treatment of Ta/Mo

Anodic oxidation used for treatment of Ta/Mo (the treated sample was labelled as Oxide/Ta/Mo). In order to prepare Oxide/Ta/Mo samples, a graphite plate was used as the cathode electrode, and a tantalum coating sample was used as the anode electrode. All samples were degreased with ethanol and then acetone to remove the contaminants on the coating surface. The treatment was performed under the following conditions, solution: 0.5 mol/L H_2SO_4, temperature: (25 ± 0.5) °C, current density: (20±0.1) $A \cdot cm^{-2}$, and anodization time: 3,600 s. During the anodization process, a water circulator was used to maintain the temperature of the electrolyte at 25 °C, and a magnetic stirrer was used to eliminate bubbles generated during the process.

2.3 Materials characterization

The surface morphology of the Ta coating was observed using field emission scanning electron microscopy (FE-SEM; Inspect F50, USA). Furthermore, the crystalline structure of the experimental sample was characterized via X-ray diffraction (XRD; D/MAX-RC Japan) using Cu-Kα radiation, a tube flow of 200 mA, a tube pressure of 40 kV, and a scanning speed of 1°/min. The data was collected through coupled continuous scanning (2θ range: 10°–100° and step: 0.02°). The thickness and changes in the valence state of the anodized film were evaluated using XPS (AXIS Ultra UK) with an Al Kα target (hν =1486.6eV) as the excitation source. An emission current of 15 mA and a voltage of 13 kV were employed. The XPS data was analyzed and processed using CASA XPS software.

2.4 Electrochemical measurements

The electrochemical measurements were performed using a CHI660E electrochemical workstation (CH Instruments, Shanghai, China). A 99.99% platinum electrode, 10 mm × 10 mm × 2 mm Ta coating, and saturated calomel electrode were used as the counter electrode, working electrode, and counter electrode, respectively. Tests were performed in an open system at a temperature of 25 ± 0.1 °C with a 3.5% NaCl solution as the electrolyte. In addition, potentiodynamic curves were recorded from -0.3 V to 0.3 V (scanning rate: 0.5 mV/s) at 25 °C. The corrosion potential (E_{corr}) and corrosion current density (i_{corr}) were determined using the Tafel extrapolation method. Furthermore, electrochemical impedance spectroscopy (EIS) measurements were performed under an open circuit potential. The differential capacitance C_{sc} of the space charge layer and the potential $\triangle\varphi$ of the surface to the body were described using the Mott-Schottky equation.

3. RESULTS AND DISCUSSION

3.1 Surface morphology and element composition of Ta coating

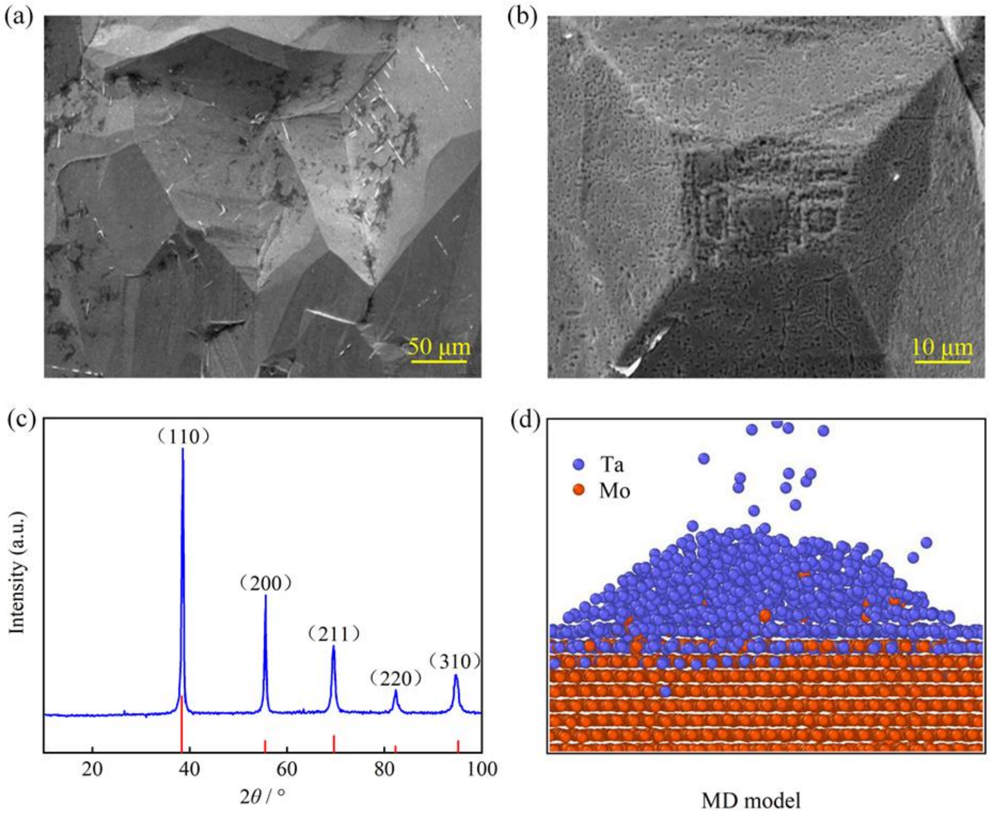

Figure 2. SEM images and XRD spectrum of Ta/Mo coating. (a) SEM image of Ta/Mo coating, (b) high magnification image of region shown in Figure 2(a), (c) XRD spectrum of Ta/Mo coating, and (d) Ta/Mo model of coating.

To determine the corrosion resistance mechanism of the Ta coating, the surface morphology and phase composition of the coating were evaluated, as shown in Figure 2. The surface morphology of the coating is characterized by island-like growth, which is typical of CVD Ta/Mo coatings. The phase composition of the coating is determined via XRD (Figure 2c), which indicates that the coating was mainly composed of α-Ta with a body-centered cubic structure, according to the relevant JCPDS card (No. 04-0788). Ta oxide is small and mainly distributed on the surface of the coating, and hence was undetected by XRD [15]. A Ta coating deposition model was constructed using molecular dynamics simulation software (Lammps) [16–18], as shown in Figure 2d. The results demonstrated that the aforementioned island-like growth induced anisotropy of the surface, and therefore sharp selective corrosion behavior was observed near the surface of the coating.

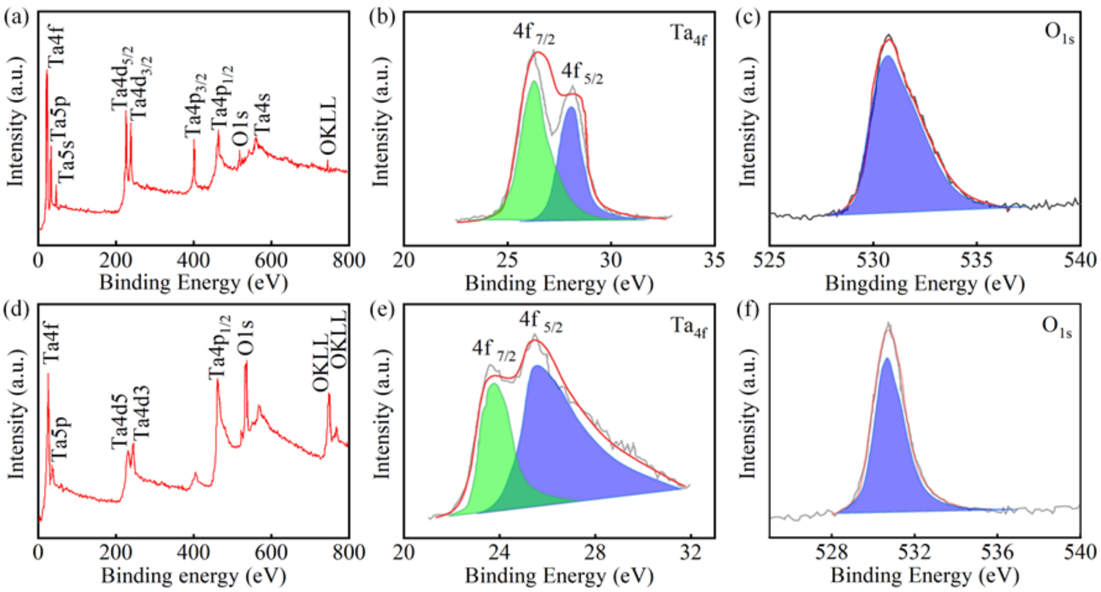

Figure 3. Results obtained via XPS of the samples. Survey spectra of the Oxide/Ta/Mo coating (a) and Ta/Mo coating (d). Narrow scan spectra of the Oxide/Ta/Mo coating (b, c) and Ta/Mo coating (e, f).

The XPS technique can be used to accurately determine the chemical composition and chemical state of a coating surface (see Figure 3 for the XPS results obtained in this work). The overall spectrum (see Figure 3 (a) and (d)) shows that the oxide film on the surface of the Oxide/Ta/Mo oxide film and Ta/Mo oxide film were composed of elemental Ta and O. The high resolution XPS spectra obtained for Ta 4f and O1s peaks were determined from the corresponding narrow spectra of the anodized films. The peaks at 26.4 eV and 28.3eV in the Ta 4f spectrum (see Figure 3(b)) were associated with Ta $4f_{7/2}$ and Ta $4f_{5/2}$, respectively, corresponding to stoichiometric Ta_2O_5 [19]. From Figure 3 (d) and (e), we observed that the four main Ta peaks correspond to Ta4f, Ta_{4d3}, $Ta4d_5$, and $Ta4p_{1/2}$. Moreover, the position of line $Ta4f_{7/2}$ in Figure 3 (e) corresponded to the typical chemical state of Ta in Ta_2O_5. Furthermore, the O1s spectrum of the natural oxide film was also analyzed, as shown in Figure 3 (c) and (f), where evidence for the existence of non-stoichiometric oxides is lacking. These results indicated that Ta_2O_5 was formed on the surface of both the Oxide/Ta/Mo and natural oxidation coatings.

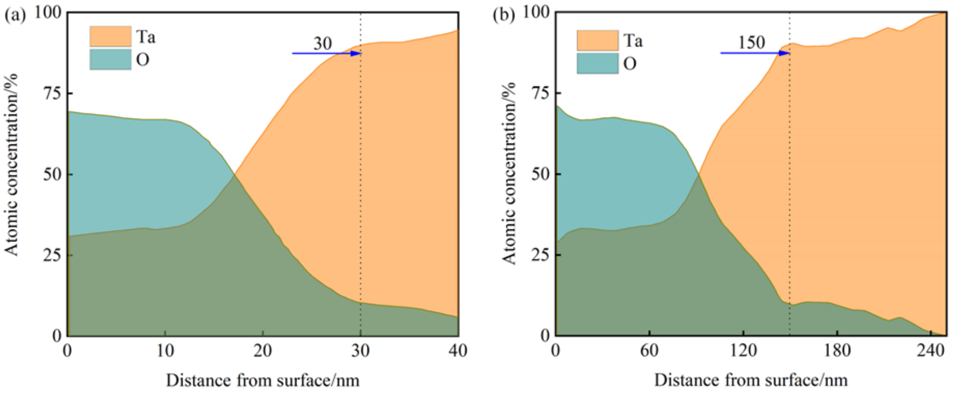

Figure 4. XPS depth profile of Ta coatings with Ta/Mo (a) and Oxide/Ta/Mo (b).

The XPS depth profile of the Ta coatings with Ta/Mo and Oxide/Ta/Mo was obtained using an electron beam at an acceleration voltage of 2 kV (see Figure 4 for the results). As shown in the figure, the Ta content increased and the oxygen content decreased with increasing depth into the film. Moreover, the oxygen diffusion layer was ~30 nm thick, and the oxygen content decreased significantly at depths of 10 nm–30 nm. This resulted in a gradient structure, thereby increasing the adhesion strength between the film and the substrate. After anodic oxidation, the thickness of the oxygen diffusion layer (~150 nm), was five times that of the natural membrane. These findings showed that an anodic oxidation treatment led to a significant increase in the thickness of the Ta oxide film, thereby improving the corrosion resistance of the coating.

3.2 Electrochemical corrosion properties of Ta coating

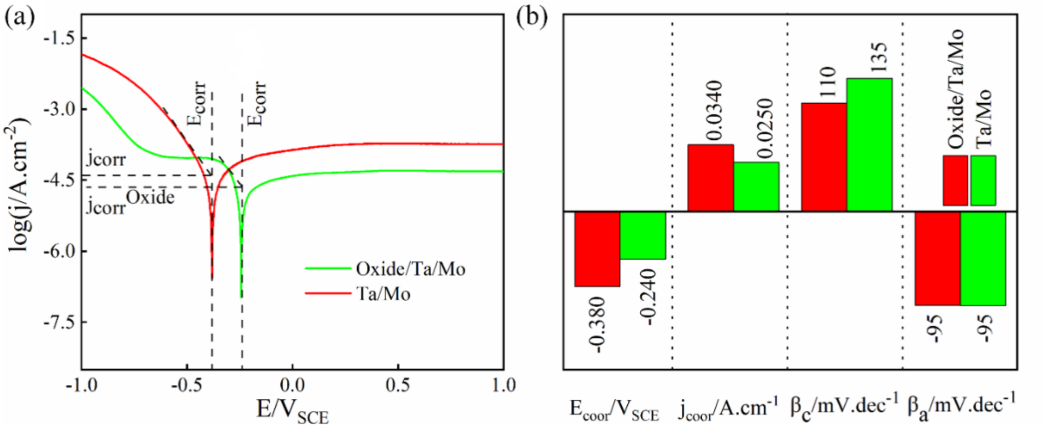

Figure 5. Potentiodynamic polarization curves of the samples with Ta/Mo and Oxide/Ta/Mo in a 3.5 wt.% NaCl solution at 25 °C.

To further investigate the corrosion resistance of the Ta coating, the electrochemical performance of the coatings was determined using a typical three electrode electrochemical workstation in a 3.5 wt.% NaCl solution at 25 °C (see Figure 5a). As shown in the figure, the samples were dissolved briefly and then passivated spontaneously, thereby inhibiting the corrosion reaction. The corrosion potential (E_{corr}) and corrosion current density (j_{corr}) of the Oxide/Ta/Mo samples were higher and lower, respectively, than those of the Ta/Mo samples. Furthermore, the corrosion resistance of the coating was improved, due to the increase in thickness and uniformity of the oxide film.

To compare the corrosion resistance of the coatings, the corrosion potential (E_{corr}), corrosion current density (j_{corr}), anodic polarization slope (βα), and cathodic polarization slope (βc) were calculated [20,21], as shown in Figure 5b. These calculations revealed that the E_{corr} of the Oxide/Ta/Mo sample was 0.140 V higher than that of the Ta/Mo sample, whereas the j_{corr} was 0.009 $A \cdot cm^{-2}$ lower. This suggests that the corrosion resistance and corrosion rate of the Oxide/Ta/Mo film were better and lower, respectively, than those of the Ta/Mo sample [22–24].

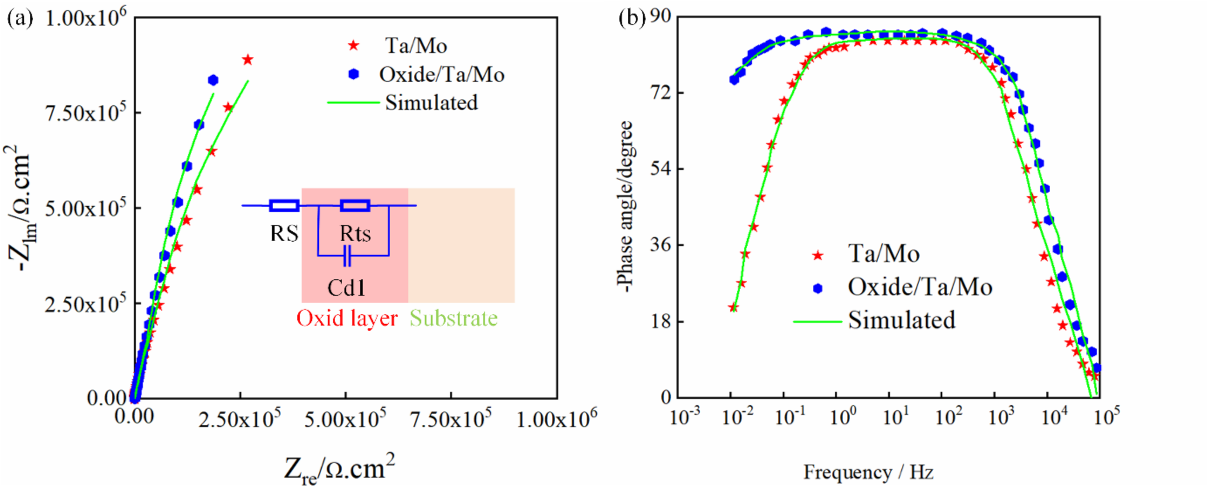

Figure 6. Nyquist (a) and Bode plots (b) of the samples with Ta/Mo and Oxide/Ta/Mo in a 3.5 wt.% NaCl solution at 25 °C.

The Nyquist and Bode plots of coatings with Ta/Mo and Oxide/Ta/Mo in an open system are shown in Figure 6. The diameter of the capacitive semicircle obtained for the Oxide/Ta/Mo coating surface was considerably larger than that of the Ta/Mo coating. As previously reported, the electron transfer resistance and the stability of the oxide film increase with increasing arc diameter; the reverse is also true [25]. Therefore, compared with the Ta/Mo coating, the oxide film of the Oxide/Ta/Mo coating had a higher electrochemical corrosion resistance and a better barrier resistance against the corrosive media. A phase angle peak of <90° occurs at frequencies of 10^0–10^3 Hz (see Figure 6b), indicating that the oxide film exhibits non-ideal capacitance behavior. After the anodization treatment, the maximum phase angle peak of the coating was close to 90°, and the range of the maximum value was maintained. This indicates that anodization is helpful in improving the stability of the oxide film, and reducing the charge transfer. These results agreed with the XPS results shown in Figure 4. The electrochemical characteristics of coatings with Ta/Mo and Oxide/Ta/Mo were investigated by calculating the impedances of the coatings using an equivalent circuit model (Figure 6a). The parameters of each circuit element after fitting are given in Table 1.

Table 1. EIS fitting circuit parameters of coatings with Ta/Mo and Oxide/Ta/Mo in 3.5 wt.% NaCl solution

Sample	Rs（Ω/cm^2）	Rct（Ω/cm^2）	Cdl($\mu F/cm^2$)
Ta/Mo	23.8	98.3×10^3	8.57×10^{-2}
Oxide/Ta/Mo	24.5	205×10^3	3.32×10^{-2}

As shown in Table 1, the Rct of the Oxide/Ta/Mo coating ($205\times10^3\ \Omega$) was more than twice that of the Ta/Mo coating ($98.3\times10^3\Omega$). The Rct value increases with increasing corrosion resistance [26]. Furthermore, we found that the Cdl values of the Ta/Mo coating and anodized coating were 3.32×10^{-2} and $8.57\times10^{-2}\ \mu F$, respectively. This implies that the passive film formed on the Oxide/Ta/Mo coating exhibited better insulating or dielectric property than that of the Ta/Mo coating. Therefore, the Oxide/Ta/Mo coating exhibited significantly higher corrosion resistance, and exerted a better protective effect than the Ta/Mo coating.

Figure 7 shows the Mott-Schottky plots of the passive films formed on coatings with Ta/Mo and Oxide/Ta/Mo. According to the Mott-Schottky theory, the space charge capacitance (Csc) of an n-type or a p-type semiconductor is given as follows [27]:

$$C_{sc}^{-2}=[2/(e\varepsilon\varepsilon_n N)](|\Delta\phi|-kT/e)=[2/(e\varepsilon\varepsilon_n N)](|E-E_{fb}|-kT/e) \qquad (3)$$

Where, Csc and ε are the space charge capacitance and the dielectric constant of the passive film, respectively. Similarly, the vacuum permittivity, elementary charge, density of the charge carriers, applied potential, flat band potential, Boltzmann constant, and absolute temperature are denoted by ε_n, e, N, E, E_{fb}, *k*, and T, respectively.

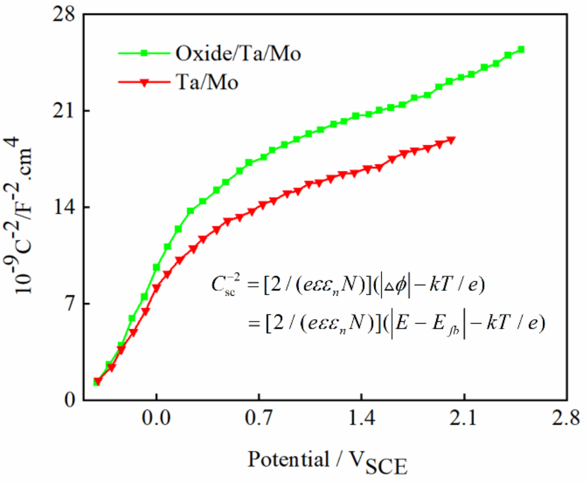

Figure 7. The Mott-Schottky plots of the passive films formed on coatings with Ta/Mo and Oxide/Ta/Mo.

The shape of the curves obtained for the Oxide/Ta/Mo coating was very similar to that of the Ta/Mo coating (see figure 7). In addition, the values of Csc^{-2} increased with increasing E_{fb}, and the slopes of both curves were always positive. The passive films formed on coatings with Ta/Mo and Oxide/Ta/Mo exhibit n-type semiconductor characteristics [28, 29]. By calculating the slope of the Mott-Schottky curve, we determine that the oxidation film of the anodized coating is more compact than that of the non-anodized coating. This increased compactness was effective in reducing the donor density of the film.

3.3 Electrochemical corrosion resistance structure model of Ta coating

The schematic presented in Figure 8 shows the electrochemical corrosion resistance of the Ta/Mo coating and Oxide/Ta/Mo coating. Simultaneous and cyclical reactions such as the formation and dissolution of the barrier layer and the formation of the porous layer occurred during the anodization process of the Ta coating. The thickness of the oxide film increased gradually when the formation rate of the new oxide film exceeded the dissolution rate. When the formation rate of the film was the same as the dissolution rate, the Oxide/Ta/Mo film was in the stable formation stage. According to the XPS depth profiles, the Oxide/Ta/Mo film (thickness: 150 nm) is approximately five times (shown in Figure 4) thicker than the Ta/Mo film. Furthermore, the Mott-Schottky curve confirmed that the compactness of the oxide film increased significantly after anodization of the film. The anodization-induced changes in the surface structure characteristics of the coating yield increased resistance against Cl^- corrosion and improved stability of the coating (shown in Figure 7), thereby extending the service life of the coating. Therefore, performance indicators, such as the thickness, compactness, and electrochemical performance was improved via anodic oxidation. This method can serve as a reference for improving the corrosion resistance of Ta coatings.

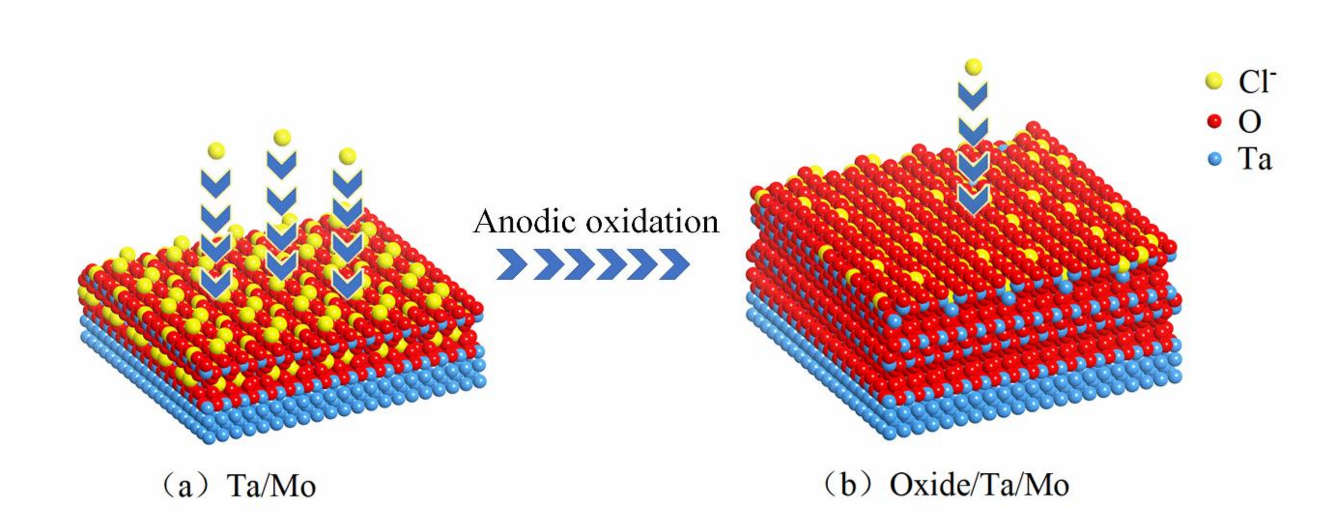

Figure 8. Schematic showing electrochemical corrosion resistance of (a) Ta/Mo and (b) Oxide/Ta/Mo.

4. CONCLUSIONS

In this work, the effect of anodic oxidation on the structure and corrosion resistance of a Ta coating was investigated. The results revealed that the Oxide/Ta/Mo film was approximately five times thicker than the natural film. The potentiodynamic polarization analysis indicated that the self-corrosion potential of the Oxide/Ta/Mo coating increased by 36.84% (from -0.38 V to -0.24 V) and the self-corrosion current density decreased by 26.47% (from 0.034 A·cm^{-2} to 0.025 A·cm^{-2}). Furthermore, the Mott-Schottky curves confirmed that the Oxide/Ta/Mo coating surface exhibited a considerably larger capacitance arc and a more compact structure than the Ta/Mo coating surface. These characteristics result in anodic oxidation and possibly a reduction in the number of channels for Cl^{-} ion transport in the film. Moreover, the results of potentiodynamic polarization and EIS measurements revealed that the electrochemical corrosion resistance of the Oxide/Ta/Mo coating was higher than that of the pre-Oxide/Ta/Mo sample. This work can serve as a reference for improving the corrosion resistance of Ta coatings prepared via CVD.

ACKNOWLEDGEMENTS

This work was supported financially by the Scientific Research Fund of Yunnan Education Department (grant Nos. 2020J0416 and 2019J0039); the National Nature Science Foundation of China (grant Nos. 52061019); Key projects of basic research plan of Yunnan Science and Technology Department (grant Nos. 202001AS070048).

References

1. M. Knezevic, J. Crapps, I. J. Beyerlein, D. R. Coughlin, K. D. Clarke and R. J. McCabe, *Int. J. Mech. Sci.*, 105(2016) 227.
2. R. Silva, M. Walls, B. Rondot, M.D.C. Belo and R. Guidoin, *J. Mater. Sci. Mater. Med.*, 13 (2002) 495.
3. Vamsi. Krishna, Balla. Shashwat and Amit. Bandyopadhyay, *Acta Biomater.*, 6 (2010) 2329.
4. G. Ma, G.Wu, W. Shi and X. Mao, *Corros. Sci.*, 176(2020) 108.
5. M. D. Bermúdez, F. J. Carrión, G. Martínez-Nicolás and R. López, Wear, 258 (2005) 693.
6. H. Asgari, M. R. Toroghinejad and M. A. Golozar, *Appl. Surf. Sci.*, 253 (2007) 6769.
7. R. Diao, J. Rong, X. Wang and X. Yu, *Int. J. Electrochem. Sci.*, 13 (2018) 7765.
8. A. Aladjem, *J. Mater. Sci. Lett.*, 8 (1973) 688.
9. Y. T Sul, C. B. Johansson, Y. Jeong and T. Albrektsson, *Med. Eng. Phys.*, 23 (2001) 329.
10. A. Afshar and M. R. Vaezi, *Surf. Coat. Technol.*, 3 (2004) 398.
11. X. Liu, P. Chu and C. Ding, *Mater. Sci. Eng. R.*, 47 (2004) 49.
12. Z.Wang, R.Diao, Z. Yuan and Z. Zhan, *Int. J. Electrochem. Sci.*, 13 (2018) 4411.
13. O. Zubillagaa, F. J. Canoa, I. Azkaratea and P. Skeldonb, *Surf. Coat. Technol.*, 203 (2009) 1494.
14. I. Milosˇev, D. Blejan, S. Varvara and L. M. Muresan, *J. Appl. Electrochem.*,43 (2013) 645.
15. X. Huang and Z. Liu, *Surf. Coat. Technol.*, 232 (2013) 224.
16. B. J. Alder and T. E. Wainwright, *J. Chem. Phys.*, 31 (1959) 459.
17. A. Rahman, *Phys. Lett. A*, 136 (1964) 405.
18. D. C. Rapaport, Cambridge University Press. 1996.
19. E. Atanassova and D. Spassov, *Appl. Surf. Sci.*, 135 (1998) 71.
20. S. Wolynec and I. Costa, *Electrochim. Acta*, 51 (2006) 1815.
21. G. Wu, K. Ding, X. Zeng and X. Wang, *Scripta Mater.*, 61 (2009) 269.
22. M. Fouladi and A. Amadeh, *Electrochimica. Acta*, 106 (2013) 106.
23. M. Carbucicchio, R. Ciprian, F. Ospitali and G. Palombarini, *Corros. Sci.*, 50 (2008) 2605.
24. H. Su and C. Lin, *Corros. Sci.*, 83 (2014) 137.
25. M. A. Khan, R. L. Williams and D. F. Williams, *Biomater. Sci.*, 20 (1999) 631.

26. H. Krawiec, V. Vignal, E. Schwarzenboeck and J. Banas, *Electrochimica. Acta*, 104 (2013) 400.
27. N. Sato, Electrochemistry at Metal and Semiconductor Electrodes, Elsevier, Amsterdam, 1998.
28. S. R. Morrison, Electrochemistry at Semiconductor and Oxidized Metal Electrodes; Plenum Press: New York, 1980.
29. W. P. Gomes and D. Vanmaekelbergh, *Electrochimica. Acta*, 41 (1996) 967.